Static Inhomogeneities in Physical Gels: Comparison of Temperature-Induced and Concentration-Induced Sol−Gel Transition

Mitsuhiro Shibayama*

Neutron Scattering Laboratory, The Institute for Solid State Physics, The University of Tokyo, Tokai, Naka-gun, Ibaraki 319-1106, Japan

Masayuki Tsujimoto, and Fumiyoshi Ikkai†

Department of Polymer Science and Engineering, Kyoto Institute of Technology, Matsugasaki, Sakyo-ku, Kyoto 606-8585, Japan

Received March 29, 2000; Revised Manuscript Received August 8, 2000

ABSTRACT: The gel−sol transition of a physical gel comprising poly(vinyl alcohol), Congo Red, and water has been studied by static/dynamic light scattering (SLS/DLS). SLS speckle patterns appeared exclusively in the gel state as observed in chemical gels (i.e., covalent bonded gels). The speckle patterns disappeared when temperature (T) was raised or concentration (C) was lowered across the temperature-induced or concentration-induced gel−sol transition point. The time−intensity correlation function obtained by DLS showed a clear transition from a power law to a stretched exponential behavior at the transition point. The transition is discussed in conjunction with the site-bond percolation theory.

Introduction

It has been recently recognized that properties of polymer gels, such as the mechanical strength,[1] viscoelasticity,[2−5] kinetics of deswelling,[6−9] and transparency,[9] depend on their spatial inhomogeneities. It was shown that the presence of spatial inhomogeneities could be simply monitored by light scattering as speckles, i.e., random fluctuations in the scattered intensity as a function of sampling points.[10,11]

In the case of chemically cross-linked polymer gels, the relationship between speckles and spatial inhomogeneities has been relatively well understood.[12] That is, chemical cross-links constrain the mobility of polymer chains in a solvent, resulting in an emergence of a nonvanishing spatial variation of refractive index. As a result, if a narrow beam of a highly coherent light, e.g., a laser beam, is irradiated to a gel, the scattered light shows random fringes called "speckles".[13] The scattering medium having nonvanishing concentration fluctuations is called a nonergodic medium and behaves as a "speckle field", where the time average is no more the same as the ensemble average. The scattering properties of such nonergodic media were extensively explored by Pusey and van Megen.[14]

Because chemically cross-linked polymer gels are usually made by copolymerizing monomers and cross-linkers, an inhomogeneous distribution of cross-linkers is introduced and spatial inhomogeneities are permanently built-in in the gel. Therefore, the degree of spatial inhomogeneities increases with increasing cross-linker concentration in the gel.[15−19] The above discussion becomes questionable if the cross-links can be attached or detached according to the chemical equilibrium of cross-linking reaction. This is the case of physical gels undergoing sol−gel transition by chemical equilibrium. In this case, it is naively expected that cross-links are distributed randomly in the space in order to minimize the conformational free energy of the network chains. Hence, physical gels may have a significantly low degree of inhomogeneities compared to chemically cross-linked gels. However, as recently reported elsewhere,[20,21] physical gels consisting of poly(vinyl alcohol)−Congo Red (PVA/CR) aqueous solutions also exhibit a high degree of inhomogeneity. The PVA/CR system was chosen as a model of physical gels because of the following reasons: (i) capability of quick gelation without hysteresis, (ii) moderate sol−gel transition temperature, T_{gel}, for easy handling (∼43 °C), and (iii) well-characterized structure and properties.[2,22,23] The presence of static inhomogeneities was verified as an appearance of speckle patterns and drastic changes in the dynamics at the sol−gel transition temperature.[21]

In this paper, we investigate the spatial inhomogeneities and dynamics of PVA/CR gels as a function of polymer concentration as well as temperature by using static/dynamic light scattering (SLS/DLS). First, we show a clear evidence for the existence of spatial inhomogeneities, i.e., an appearance of speckle patterns, in a series of PVA/CR gels having different concentrations. Then, the dynamics of PVA/CR aqueous systems near the sol−gel transition threshold is extensively discussed by analyzing speckle patterns and intensity correlation function (ICF). It will be emphasized that the concentration-induced sol−gel transition is different from the temperature-induced sol−gel transition. The correlation length, ξ, diverges at the transition in the case of concentration induced sol−gel transition, while a continuous change in ξ is observed for temperature-induced transition. The physical implementation of the difference will be made in terms of the concept of the site-bond percolation theory.[24]

Theoretical Section

1. Time−Intensity Correlation Function. The time−intensity correlation function (ICF), $g_T^{(2)}(\tau)$, is defined by

* To whom correspondence should be addressed.
† Present address: The Institute of Advanced Science Research, L'ORÉAL Tsukuba Center, 5-5 Tokodai, Tsukuba, Ibaraki 300-2635, Japan.

10.1021/ma000563v CCC: $19.00
Published on Web 09/28/2000

$$g_T^{(2)}(\tau) = \frac{\langle I(t)\, I(t+\tau)\rangle}{\langle I(t)\rangle_T^{\,2}} \quad (1)$$

where $I(t)$ and $I(t+\tau)$ indicate the scattered intensities at time t and $t+\tau$, respectively. The subscript T denotes time averaging. In the case of polymeric systems undergoing gelation, the intensity correlation function, $g_T^{(2)}(\tau)$, can be often given by the square of the sum of two terms representing fast and slow modes.[25] The fast mode is the cooperative diffusion of chain molecules. On the other hand, the slow mode corresponds to the translational diffusion of clusters (in the sol state) or an internal cooperative diffusion in infinite clusters (in the gel state). Hence, $g_T^{(2)}(\tau)$ can be written as[26−28]

$$g_T^{(2)}(\tau) - 1 \approx \{A \exp(-D_A q^2 \tau) + (1 - A) \exp[-(\tau/\tau_{slow})^{\beta}]\}^2 \text{ (for sols)} \quad (2)$$

$$g_T^{(2)}(\tau) - 1 \approx \{A \exp(-D_A q^2 \tau) + (1 - A)[1 + (\tau/\tau^*)]^{(n-1)/2}\}^2 \text{ (for gels)} \quad (3)$$

where D_A, q, and τ denote the apparent diffusion coefficient of the fast mode, the scattering vector, and the relaxation time, respectively. A is the fraction of the fast mode. τ_{slow} is the characteristic decay time for the slow mode, and β is the stretched exponent. τ^* is the characteristic time where the power law behavior appears, and n ($0 < n < 1$) is the fractal dimension of scattered photons.[28]

2. Decomposition of the Scattered Intensity to Two Components from Thermal Fluctuations and Static Inhomogeneities. For a nonergodic medium like a gel, it is known that the value of D_A depends on the sampling points in the range of $D/2 < D_A < D$. D is the cooperative diffusion coefficient, which reflects the mobility of the chain molecules in the sample, and is given by[14,29,30]

$$g_T^{(2)}(\tau) - 1 = X^2 \exp(-2Dq^2\tau) + 2X(1 - X) \exp(-Dq^2\tau) \text{ (for } \tau \ll \tau^*) \quad (4)$$

where X ($=\langle I_F\rangle_T/\langle I\rangle_T$) is the ratio of the intensity from the time-fluctuating component, $\langle I_F\rangle_T$, to the total intensity, $\langle I\rangle_T$, at a given sampling point. The apparent diffusion coefficient was evaluated by the initial slope of ICF, i.e.,

$$D_A = -\frac{1}{2q^2}\frac{\partial}{\partial\tau} \ln[g_T^{(2)}(\tau) - 1]|_{\tau=0} \quad (5)$$

Note that D_A is sampling-point-dependent if the system is in the gel state. Equations 4 and 5 lead to the following relationship:[29]

$$D_A = \frac{D}{2 - \langle I_F\rangle_T/\langle I\rangle_T} \quad (6)$$

Hence, one can evaluate D and $\langle I_F\rangle_T$ by fitting observed ICFs with eq 6 or by plotting $\langle I\rangle_T/D_A$ vs $\langle I\rangle_T$:[18,31]

$$\frac{\langle I\rangle_T}{D_A} = \frac{2}{D}\langle I\rangle_T - \frac{\langle I_F\rangle_T}{D} \quad (7)$$

Experimental Section

Samples. A series of poly(vinyl alcohol)−Congo Red (PVA−CR) aqueous solutions were prepared. PVA powder (degree of polymerization = 1800 and degree of saponification = 99.96 mol %), kindly supplied by Nippon Gosei Co. Ltd., Osaka, Japan, was used without further purification. CR ($C_{32}H_{22}N_6Na_2O_6S_2$) was purchased from Wako Chemical Co. Ltd., Tokyo. CR is a synthetic dye and is known as a thermoreversible cross-linker of PVA in aqueous solutions.[32] The cross-linking mechanism is discussed elsewhere.[33] Both 1.36 M PVA and 20 mM CR aqueous solutions were separately prepared by dissolving them in boiling distilled water and filtering through a 0.45 μm filter. Equal amounts of two solutions were mixed together at ca. 80 °C, and a homogeneous solution of PVA−CR with C_{PVA}/C_{CR} = 680 mM/10 mM was obtained, where C_{PVA} and C_{CR} are concentrations of PVA in monomeric unit and of CR, respectively. The sol−gel transition temperature for C_{PVA}/C_{CR} = 680 mM/10 mM was determined to be 43 °C by flow measurement, which is in good agreement with the sol−gel phase diagram for PVA/CR aqueous systems reported elsewhere.[22] Figure 1 shows the sol−gel phase diagram for PVA/CR aqueous solutions obtained at 20 °C. The system with C_{PVA}/C_{CR} = 680 mM/10 mM is denoted by the filled circle. To investigate concentration dependence of the sol−gel behavior, both PVA and CR concentrations were varied by keeping the molar ratio. The sets of concentrations employed for dynamic light scattering experiments were varied from C_{PVA}/C_{CR} = 114 mM/1.67 mM to 795 mM/11.7 mM as indicated by open circles in Figure 1.

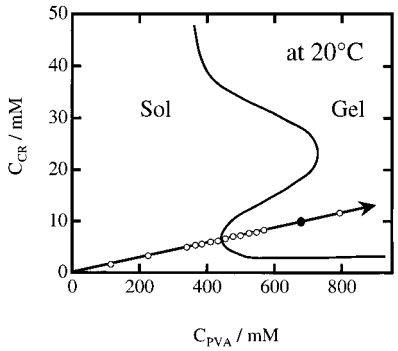

Figure 1. Phase diagram of the PVA/CR aqueous system at 20 °C. The open and filled circles denote the concentrations of PVA and CR studied in this work.

SLS/DLS. Static and dynamic (SLS and DLS) light scattering experiments were carried out on a DLS/SLS-5000 (ALV, Co Ltd., Langen, Germany) with a 22 mW He−Ne laser (wavelength, λ = 6328 Å). The sample in a 10 mm test tube was placed in a toluene bath thermostated within an error of ±0.1 °C. The time-averaged scattered intensity, $\langle I\rangle_T$, and its time correlation, i.e., the time-averaged intensity correlation, $\langle I(t)I(t+\tau)\rangle_T$, were taken at the scattering angle of 90°. The measurements were repeated at 100 different sampling points per sample at 20 °C in order to obtain ensemble average for each sample having different C_{PVA}'s. The temperature-dependent measurements were also conducted at temperatures of 20, 24, 29, 34, 38, 43, 48, 52, and 57 °C for the gel with C_{PVA}/C_{CR} = 680 mM/10 mM. Whenever the temperature was changed, at least 30 min was posed before starting the next DLS/SLS experiment in order to make sure thermal stabilization.

Results and Discussion

1. Speckle Pattern. Figure 2a shows the variations of $\langle I\rangle_T$ with sampling points obtained at different C_{PVA}'s. Here, the sampling points were chosen arbitrarily by rotating the test tube containing the sample. For $C_{PVA} \le 432$ mM, $\langle I\rangle_T$ does not depend on sampling points, indicating that the system is ergodic. On the other hand, $\langle I\rangle_T$ becomes nonergodic for $C_{PVA} > 455$ mM. The nonergodicity is verified as an appearance of speckle patterns, i.e., strong fluctuations in $\langle I\rangle_T$ with sampling points. The horizontal solid and dashed lines in the figure indicate the ensemble average of the scattered

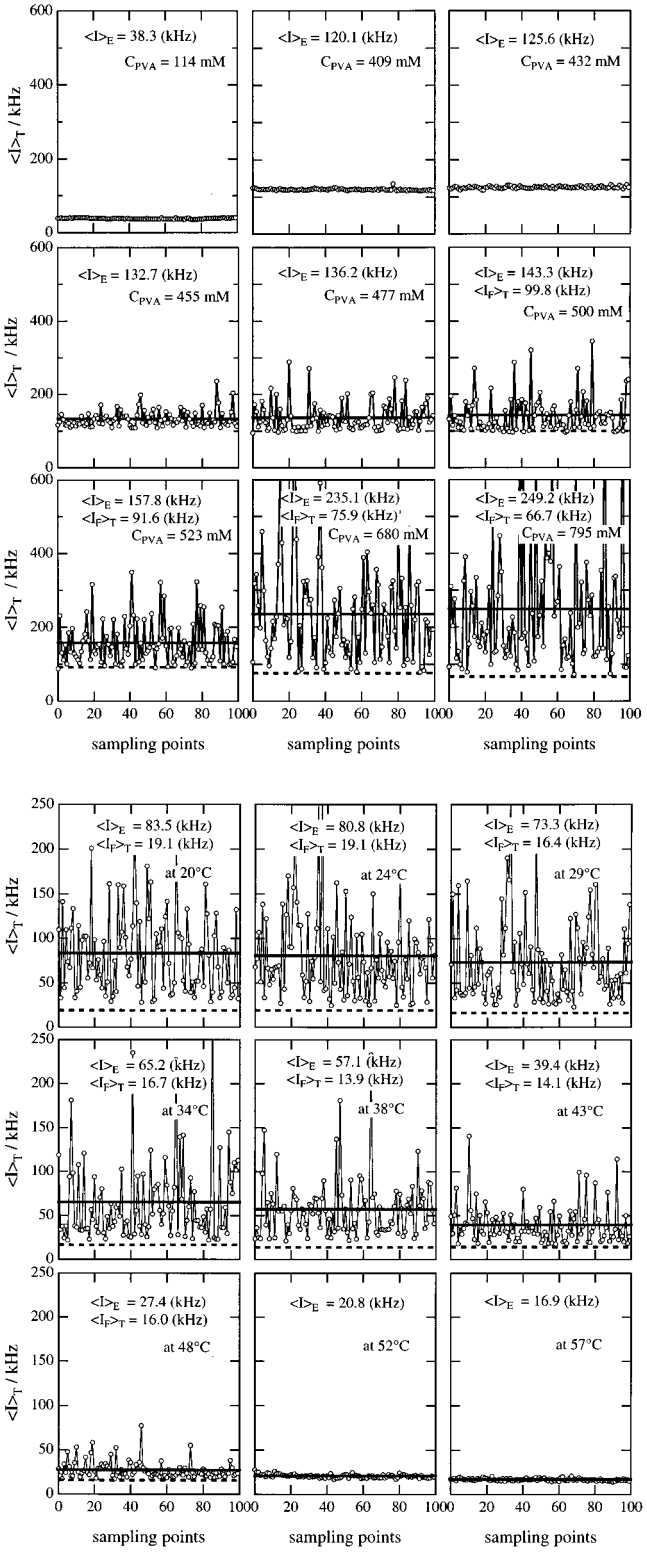

Figure 2. Variation of the scattered intensity, $\langle I \rangle_T$, with sampling points. (a, upper) Concentration and (b, lower) temperature dependence. The solid and broken line indicate the ensemble average scattered intensity, $\langle I \rangle_E$, and the fluctuating component of the scattered intensity, $\langle I_F \rangle_T$, respectively.

intensity, i.e., $\langle I \rangle_E \equiv \langle \langle I \rangle_T \rangle_E$, and the dynamic component of the scattered intensity, $\langle I_F \rangle_T$, respectively, where the subscript E denotes ensemble average. The latter reflects the solution-like fluctuations evaluated by the method described in the theoretical section. It is needless to mention that the annihilation of speckles at $C_{PVA} \approx 432$ mM is ascribed to the sol−gel transition (see Figure 1). A similar behavior in the appearance/disappearance of speckle patterns was observed for the PVA/CR(680 mM/10 mM) system by changing temperature as shown in Figure 2b. The speckles decrease by increasing temperature and completely disappear above 52 °C. Hence, frozen inhomogeneities similar to those in chemical gels are confirmed to be also present in physical gels, e.g., the PVA/CR aqueous system in the gel state.

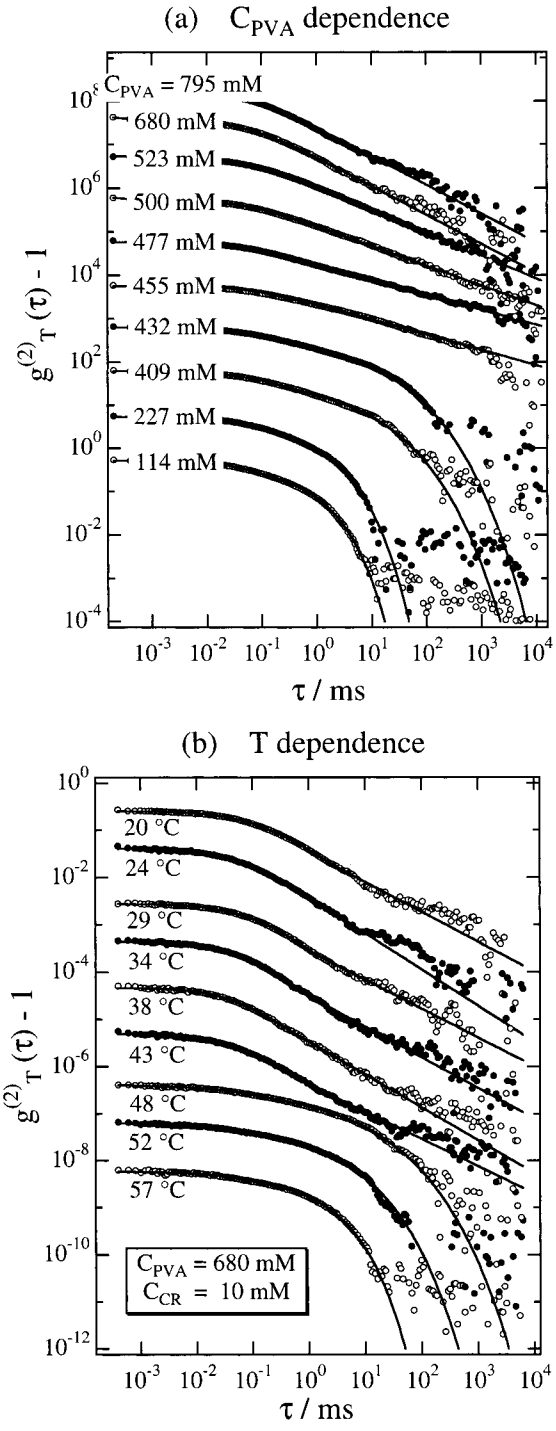

Figure 3. Time−intensity correlation function, $g_T^{(2)}(\tau)$, for PVA/CR aqueous systems (a) at different C_{PVA}'s and (b) at different temperatures, T. To avoid overlap, $g_T^{(2)}(\tau)$'s are shifted vertically as C_{PVA} or T increases. The solid lines are the results of curve fitting with a stretched exponential function (eq 2) and with a power law function (eq 3).

2. Intensity Correlation Function. Figure 3a shows a series of intensity correlation functions (ICF's), $g_T^{(2)}(\tau)$, for PVA/CR systems with different C_{PVA}'s obtained at 20 °C. The ICF's, except for that for C_{PVA} = 114 mM, were shifted vertically upward with the step of 1 order of magnitude each to avoid overlap. As clearly shown in the figure, $g_T^{(2)}(\tau)$ changes drastically between C_{PVA} = 432 and 455 mM. Since the sol−gel transition threshold is known to be located around C_{PVA} = 455 mM by a flow measurement, it is clear that this dramatic change in $g_T^{(2)}(\tau)$ definitely corresponds to the macroscopic change in the flow behavior from a sol ($C_{PVA} \leq$ 432 mM) to a gel ($C_{PVA} \geq$ 455 mM). The observed ICFs were fitted with a stretched-exponential function for sols (eq 2) or a power-law function for gels (eq 3), and the fitting results are quite satisfactory as shown with the solid lines in the figure.

Figure 3b shows the series of ICFs obtained for PVA/CR (680 mM/10 mM) at different temperatures. The gel−sol transition is again clearly suggested as a change of the shape of ICF between 43 and 48 °C. For T < 43 °C, the ICF's are well represented by the power-law function (eq 3). On the other hand, the functional form of the ICF suddenly changes to a stretched exponential function at 48 °C and remains to be the same for T > 48 °C. These results clearly indicate that the dynamics changes drastically at the sol−gel transition temperature. It is interesting to analyze the ICF's as a function of C_{PVA} and T more quantitatively in terms of the fitting parameters, which are done in the following sections.

3. Evaluation of the Correlation Length and Decomposition of the Scattered Intensity. First, let us focus on the fast mode, so-called the gel mode[34] and estimate the correlation length, ξ. The gel mode corresponds to the chain dynamics in a concentration blob, where the spatial correlation exists.[35] Hence, the gel mode can be observed not only in a gel but also in a semidilute polymer solution where concentration blobs are in contact with each other.[12] Figure 4 shows the plots of $\langle I\rangle_T/D_A$ as a function of $\langle I\rangle_T$ for the PVA−CR as a function of (a) C_{PVA} and (b) T, where a is a horizontal shift factor introduced to avoid overlap. The solid lines are the fits with eq 7. It is clear from the plots that the slope of the fit decreases with increasing C_{PVA}. This indicates that D (the inverse of the slope) increases significantly with increasing C_{PVA}. Surprisingly, such a notable change is not observed when temperature is scanned (see Figure 4b). When a gel melts and becomes a sol (i.e., an ergodic medium), all data points are expected to collapse at a single point $D_A = D$ in the plot of $\langle I\rangle_T/D_A$ vs $\langle I\rangle_T$, which in fact happens at T = 57 °C. It should be noted the following. Since eq 7 could not be applied for sols, we simply took arithmetic average of D_A for the following discussion. The values of D, evaluated at scattering angles of 40°−140°, were identical within the experimental error, suggesting that the fast mode was diffusive.

Figure 5 shows the (a) C_{PVA} dependence and (b) T dependence of the correlation length, ξ, obtained from the fast mode of ICF with

$$\xi = \frac{k_B T}{6\pi\eta D} \tag{8}$$

where k_BT and η denote the Boltzmann energy and the solvent viscosity, respectively. Note that ξ indicates the size of concentration blobs. The dotted lines in the figures indicate (a) $C_{PVA,gel}$ (≈432 mM) and (b) T_{gel} (≈43 °C) obtained by a flow measurement. Interestingly, the variation of ξ with C_{PVA} (Figure 5a) is quite different from that with T (Figure 5b) from the following points of view. When C_{PVA} is scanned, ξ exhibits a maximum

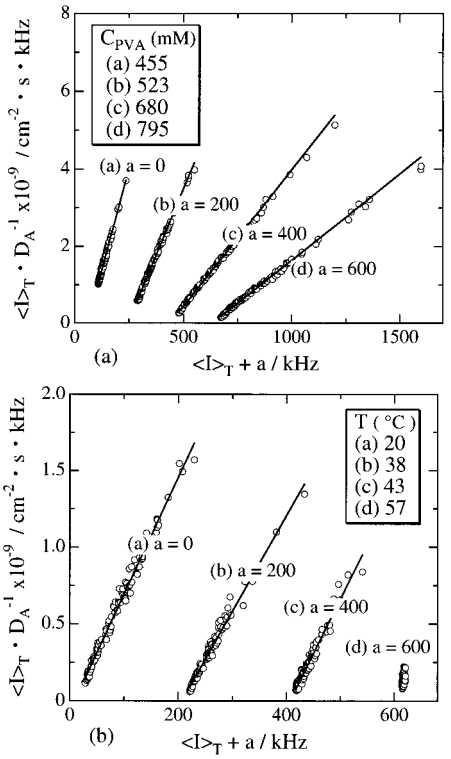

Figure 4. (a) Plots of $\langle I\rangle_T/D_A$ as a function of $\langle I\rangle_T$ for PVA/CR with various C_{PVA}'s at T = 20 °C. (b) Plots of $\langle I\rangle_T/D_A$ as a function of $\langle I\rangle_T$ for PVA/CR with various T's. The symbol a is a horizontal shift factor introduced to avoid overlap. The solid lines are the fits with eq 7.

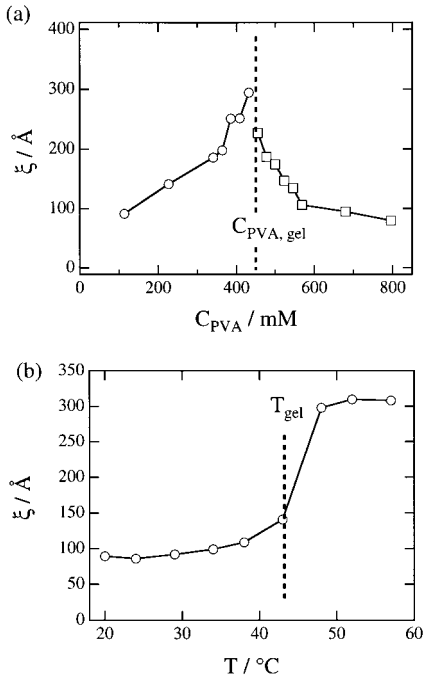

Figure 5. (a) C_{PVA} dependence and (b) T dependence of the correlation length, ξ. The dashed lines indicate the sol−gel transition concentration and temperature, respectively, obtained by the flow test.

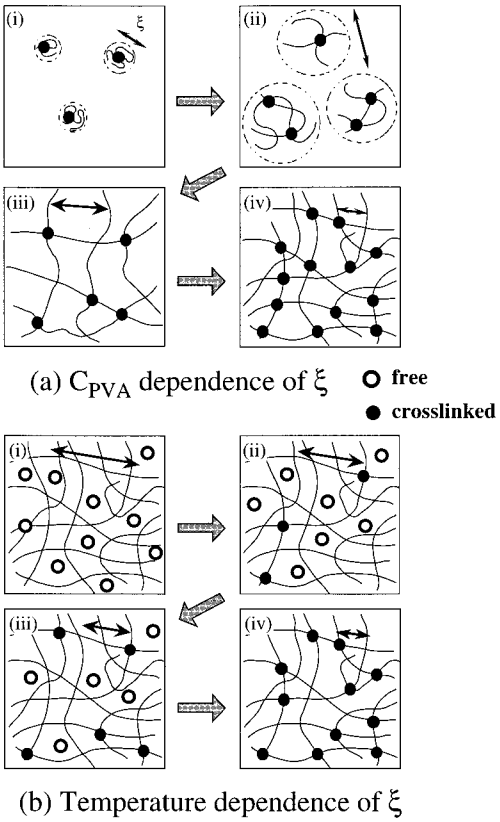

Figure 6. Illustrations explaining the C_{PVA} and T dependence of ξ. C_{PVA} increases but T decreases from (i) to (iv). Open and filled circles denote free and cross-linked CR molecules. The arrows in the figures indicate the length of ξ.

at $C_{PVA,gel}$. In contrast to the C_{PVA}-induced sol−gel transition, ξ is a monotonic increasing function of T, and no anomaly is observed at T_{gel}.

The reasons for the difference in the variations of ξ can be discussed with schematic illustrations in Figure 6. In the concentration regime of $C_{PVA} < C_{PVA,gel}$ (i), the PVA chains do not percolate yet and form "microgels". In this regime, translational diffusion of microgel clusters is observed by DLS. Therefore, the increase in ξ is due to an increase of cluster size with C_{PVA} ($<C_{PVA,\,gel}$) and ξ diverges at $C_{PVA,\,gel}$ due to volume filling by PVA clusters (ii). The following decrease in ξ for $C_{PVA} > C_{PVA,gel}$ corresponds to a decrease in blob size by further increase in C_{PVA} (iii to iv). In contrast to the concentration-induced sol−gel transition, the temperature-induced sol−gel transition is governed by chemical equilibrium of complexation of CR with PVA. In the bottom figures, active CR molecules participating in cross-linking are shown with filled circles, while free CR molecules are denoted by open circles. As shown in the figures, a decrease in temperature (i to iv) results in activation of cross-link formation. Therefore, the mesh size becomes smaller by decreasing T. In this process, no anomaly is expected in the spatial correlation, while the connectivity correlation may diverge at the sol−gel transition.[36] However, if the concentration of polymers is high enough to screen the dynamic correlation between neighboring concentration blobs, no anomaly is expected at the sol−gel transition point. This is what happens in the temperature-induced sol−gel transition. Hence, a monotonic decrease in ξ is observed by decreasing T without divergence in ξ at T_{gel}.

Figure 7a,b shows the variations of $\langle I\rangle_E$ and $\langle I_F\rangle_T$ as a function of (a) C_{PVA} and (b) T. These quantities were

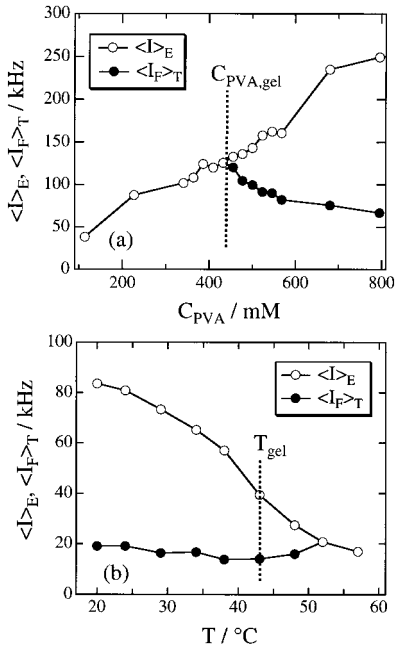

Figure 7. (a) C_{PVA} dependence and (b) T dependence of $\langle I\rangle_E$ and $\langle I_F\rangle_T$. The dashed lines indicate the sol−gel transition concentration and temperature, respectively.

evaluated by analyzing position-dependent scattered intensity and the corresponding correlation functions obtained at 100 sampling points for each sample with eq 7. As is shown, $\langle I\rangle_E = \langle I_F\rangle_T$ for $C_{PVA} \le C_{PVA,gel}$, but they split for $C_{PVA} > C_{PVA,gel}$. It is noteworthy that $\langle I\rangle_E$ increases with C_{PVA}, while $\langle I_F\rangle_T$ decreases. In this work, we varied C_{PVA} by keeping the ratio of C_{PVA} and C_{CR}. Hence, an increase in $\langle I\rangle_E$ with C_{PVA} is naively expected due to an increase in the degree of inhomogeneities with increasing in C_{CR}. On the other hand, the decrease in $\langle I_F\rangle_T$ for $C_{PVA} > C_{PVA,gel}$ is explained as follows.

In the case of semidilute polymer solutions, the scattered intensity due to thermal fluctuations, i.e., $\langle I_F\rangle_T$, is given by[34]

$$\langle I_F\rangle_T \sim k_B T C\left(\frac{\partial \Pi}{\partial C}\right)^{-1} \tag{9}$$

where C is the number concentration of the monomer constituting polymers and Π is the osmotic pressure. Π is given by[35]

$$\Pi = \frac{k_B T}{\xi^3} \tag{10}$$

Hence, one expects that

$$\langle I_F\rangle_T \sim C^{-1/4} \tag{11}$$

In deriving eq 11, one of the scaling relations for semidilute polymer solutions, $\xi \sim C^{-3/4}$, was used. Therefore, the theory predicts a gradual decrease in $\langle I_F\rangle_T$ with C_{PVA} ($\sim C$), which is indeed observed in the PVA/CR systems. A similar result was also obtained in chemically cross-linked poly(*N*-isopropylacrylamide) gels.[37]

When temperature is scanned, $\langle I_F\rangle_T$ (thermal fluctuations) is expected to change in proportion to the absolute temperature, i.e., T. The experimental data are not

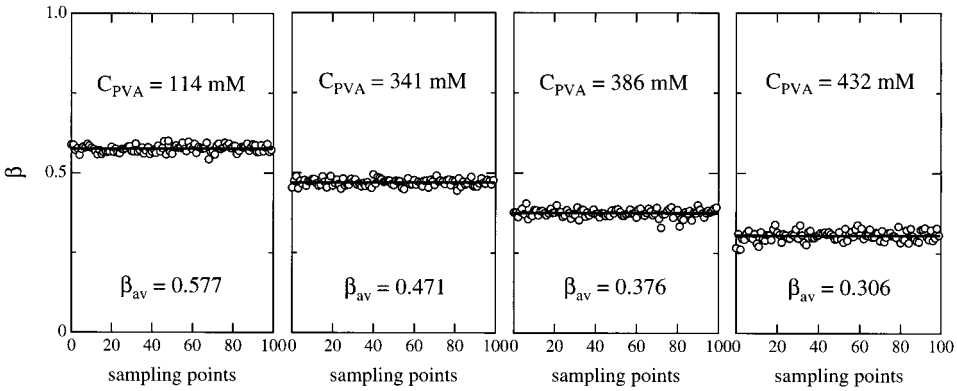

Figure 8. Variation of the stretched exponent, β, with sampling points for $C_{PVA} < C_{PVA,gel}$. The solid line in the figure shows the average value for 100 sampling points, β_{av}.

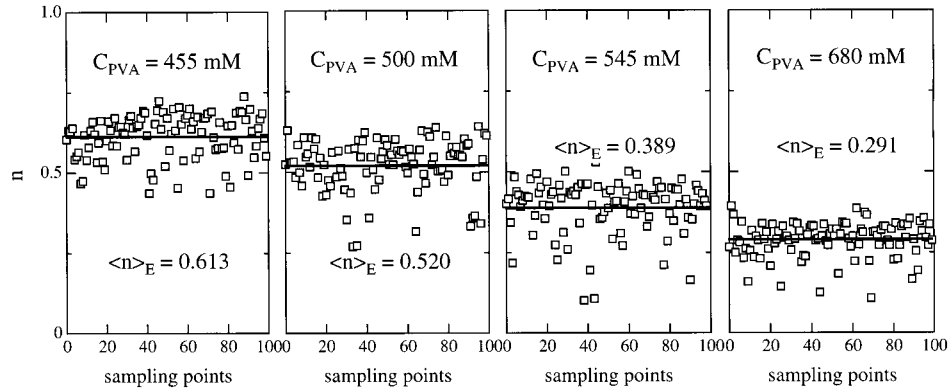

Figure 9. Variation of the power-law exponent, n, with sampling points for $C_{PVA} > C_{PVA,gel}$. The solid line in the figure shows the ensemble average of n for 100 sampling points, $\langle n \rangle_E$.

precise enough to detect such a change in this temperature range. This is why $\langle I_F \rangle_T$ does not change noticeably as shown in Figure 7b. On the other hand, $\langle I \rangle_E$ is a strongly decreasing function of T as a result of progressive scission of cross-links with T. Another interesting feature is that the bifurcation temperature is different from T_{gel}. This may be ascribed to the nature of ill-posed transition for the temperature induced sol−gel transition as discussed in Figure 5.

Rigorously speaking, the decomposition method employed above can be applied only for the case where the fast mode is clearly separated from the slow mode (i.e., the case of $0 \ll A < 1$), such as the case of chemical gels prepared by chemical cross-linking.[31] In the case of the PVA/CR gels, on the other hand, the contribution of the fast mode was found to be relatively weak. Hence, we employed an alternative method to evaluate $\langle I_F \rangle_T$. We took an ensemble average of the time-average correlation function $g^{(2)}_{T,p}(\tau)$ over many sampling points, p. The ensemble average second-order correlation function, $g^{(2)}_E(\tau)$, and the field correlation functions, $g^{(1)}_E(\tau)$, are defined by

$$g^{(2)}_E(\tau) \equiv \frac{\sum_p \langle I(0)\, I(\tau) \rangle_{T,p}}{\sum_p \langle I(0) \rangle_{T,p}^2} = \frac{\sum_p \langle I(0) \rangle_{T,p}^2 g^{(2)}_{T,p}(\tau)}{\sum_p \langle I(0) \rangle_{T,p}^2} \quad (12)$$

$$g^{(1)}_E(\tau) \equiv \sqrt{g^{(2)}_E(\tau) - 1} \quad (13)$$

The time-fluctuating component in the scattered intensity, $\langle I_F \rangle_T$, is given by

$$\langle I_F \rangle_T = \langle I \rangle_E [1 - g^{(1)}_E(\tau \to \infty)] \quad (14)$$

The variations of the evaluated $\langle I_F \rangle_T$ as a function of both C_{PVA} and T were found to be quite similar to those obtained with eq 7 respectively for the C_{PVA} and T. Therefore, we conclude that the findings shown in Figure 7 are universal phenomena for thermoreversible polymer gels.

4. Analysis of the Stretched Exponential and the Power-Law Exponent. Regarding the slow mode, we found two types of dynamics characterized by either a stretched exponential or a power law functions (see Figure 3). The former appears in the sol state, i.e., either at low concentrations ($C_{PVA} < C_{PVA,gel}$) or at high temperatures (i.e., $T > T_{gel}$), while the latter is found in the gel state. Those are characterized by the stretched exponent, β and the exponent, n. Figure 8 shows the stretched exponent, β (open circles), for sols with $C_{PVA} \leq 432$ mM obtained at various sampling points. As shown here, the value of β does not depend on the sampling points and is a decreasing function of C_{PVA}. Since the system is ergodic, the invariance of β with sampling points is reasonable. Therefore, in the following discussion, we simply take arithmetic average of β and call β_{av}.

Above $C_{PVA,gel}$ ($\approx$455 mM), all ICF's show a power law behavior. Figure 9 shows the distribution of the exponent, n (open squares). In contrast to the case of β in Figure 8, the values of n are highly scattered with sampling points. We propose here a hypothesis: A piece of gel consists of an assembly of uncorrelated domains

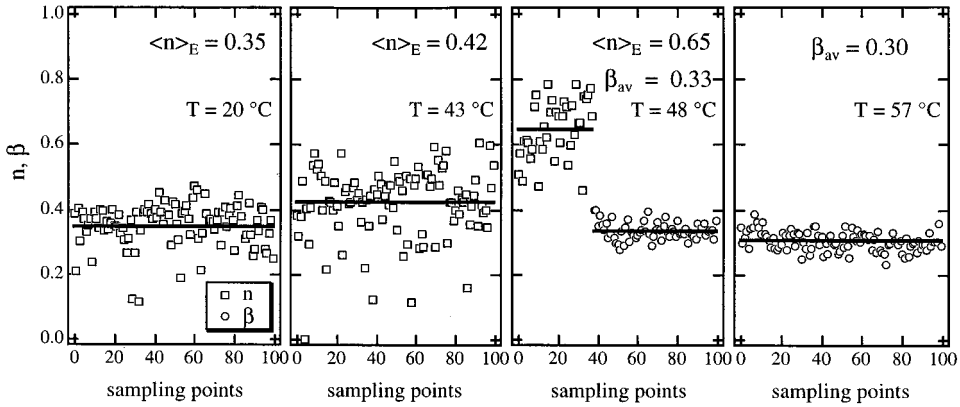

Figure 10. Plots showing fluctuations of n and β. Note that at $T = 48$ °C there exist two types of correlation functions fitted with either a power-law or a stretched-exponential function. These correspond to a gel and sol phase, respectively, and $\langle n \rangle_E$ and β_{av} are obtained.

in which the connectivity correlation exists. The characteristic size of domains, Ξ, is much larger than the concentration blob in which the spatial correlation exists. We also allow the uncorrelated domains to have different degrees of inhomogeneities. Hence, the uncorrelated domains are characterized by Ξ and n. In this case, a laser light scattering study with a fine size of the incident beam may provide a sampling-point-dependent correlation function, provided Ξ being larger than the focal size of the incident beam at the sample. This criterion is satisfied in this work since speckle patterns are really observed in the PVA/CR gels. Consequently, the values of n are fluctuated with sampling points, and one needs to take an ensemble average n, i.e., $\langle n \rangle_E$. The solid line in the figure shows $\langle n \rangle_E$ obtained by averaging over the 100 sampling points. $\langle n \rangle_E$ decreases gradually with increasing C_{PVA}, from 0.613 to 0.291. It is known that the value of n decreases with increasing screening effect.[38] Hence, this result indicates that the hydrodynamic as well as excluded-volume screening effects becomes stronger with C_{PVA}.

Similar results were obtained for PVA/CR gels by varying temperature as shown in Figure 10. However, it should be noted that both types of dynamics, i.e., sol- and gel-type dynamics given by eqs 2 and 3, coexist in one sample at 48 °C. Here, the order of data points are rearranged to the regions for evaluation of n (left) and β (right). As shown in the figure, the fractions of gel and sol states in the system are estimated to be about 40% and 60%, respectively. Though the sample at 48 °C was seemingly a sol by flow test, a characteristic feature of gels, i.e., a power law behavior, is also observed as well with the probability of about 40%. When $\beta_{av} = 0.33$ appears at 48 °C, $\langle n \rangle_E$ increases drastically to 0.65. The physical meaning of this behavior is unclear at this stage. For $T > 48$ °C, the power law behavior disappears completely, and all ICFs sampled at different sampling points could be fitted with a stretched exponential function with $\beta_{av} = 0.3$.

Figure 11a shows the variations of $\langle n \rangle_E$ and β_{av} with C_{PVA}. As shown in the figure, β_{av} decreases with increasing C_{PVA} ($< C_{PVA,gel}$). This means that the ICF becomes highly stretched by approaching $C_{PVA,gel}$. Accordingly, the characteristic time for the slow mode, τ_{slow} exhibits a tendency to diverge by approaching $C_{PVA,gel}$. For $C_{PVA} > C_{PVA,gel}$, $\langle n \rangle_E$ can be estimated, and it decreases with C_{PVA}, indicating that the excluded-volume screening effect becomes stronger with increasing C_{PVA}. In the case of the temperature dependence

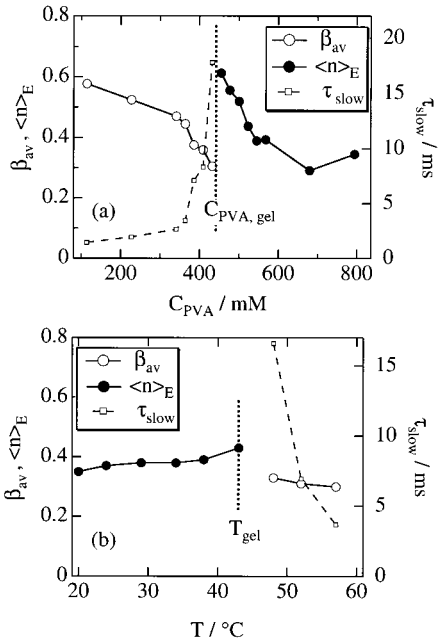

Figure 11. (a) C_{PVA} dependence and (b) T dependence of $\langle n \rangle_E$ and β_{av}. The variation of the τ_{slow} is also plotted with the right axis for the sol state.

(Figure 11b), the variations of β_{av} and $\langle n \rangle_E$ are different from the case of the C_{PVA} dependence. For example, the changes of β_{av} and $\langle n \rangle_E$ with T seem to be much less than those with C_{PVA} dependence except for τ_{slow}. τ_{slow}, on the other hand, seems to diverge as $C_{PVA} \rightarrow C_{PVA,gel}$ and $T \rightarrow T_{gel}$. Note that a tendency of divergence of τ_{slow} is also reported in a temperature-induced sol−gel transition of gelatin by Ren et al.[26] The invariance of β_{av} and $\langle n \rangle_E$ may be explained as follows. In the case of the T dependence, only the number of active cross-linkers changes with T by keeping the total concentration C_{PVA} and C_{CR} constant as schematically depicted in Figure 6b. In addition, the excluded volume does not change significantly with T for PVA aqueous systems in this temperature range, resulting in an invariance of β_{av} and $\langle n \rangle_E$ against T. When C_{PVA} (and C_{CR}) is varied, on the other hand, the system changes from a dilute solution to a semidilute solution for $C_{PVA} > C_{PVA,gel}$. Therefore, the excluded volume decreases with increasing C_{PVA}. This means an increase in the degree of excluded-volume screening. This is the reason why $\langle n \rangle_E$ decreases with C_{PVA}.

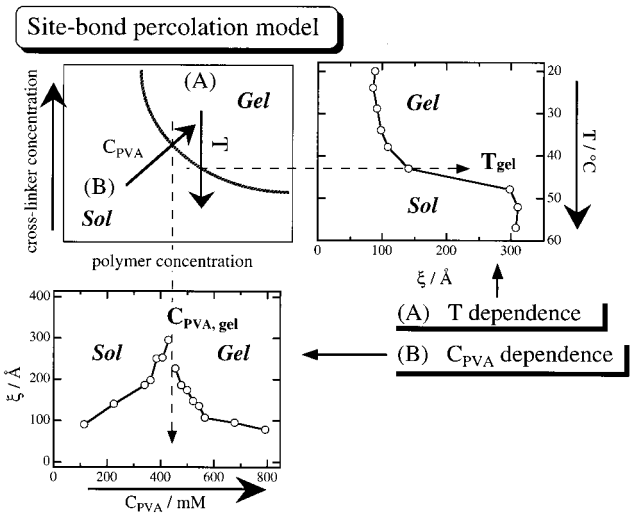

Figure 12. Schematic representation of the site-bond percolation phase diagram, which explains the (A) temperature and (B) C_{PVA} dependence of ξ.

The top-left figure in Figure 12 illustrates a phase diagram based on the site-bond percolation proposed by Coniglio et al.[24] The ordinate and abscissa denote the bond probability and site probability, which correspond to the cross-link concentration and polymer concentration, respectively. Since the cross-link concentration decreases with increasing T, an increase in the bond probability means an decrease in T. The variations of ξ with (a) T and (b) C_{PVA} discussed in Figure 5 are also shown in the right and bottom figures, respectively. These figures clearly show that site percolation is different from bond percolation. A continuous variation of ξ is observed in the case of the temperature-induced sol−gel transition, and no anomaly is observed at T_{gel} as shown in (A). On the other hand, a cusplike transition in ξ is involved in the concentration-induced sol−gel transition (B), which is due to the crossover of the so-called chain overlap concentration. The correlation length becomes largest at this concentration and undergoes a connectivity transition from unpercolated to percolated clusters. In the case of the temperature-induced sol−gel transition, the transition is simply manifested by a switching on and off of cross-links (Figure 6b). Hence, the correlation length varies smoothly across the sol−gel transition temperature. This is why no characteristic change in the temperature-induced sol−gel transition has been observed in thermoreversible polymer gels. We believe that the results disclosed here provide an important aspect of the sol−gel transition and the nature of connectivity transition.

Conclusions

We have investigated the spatial inhomogeneities in thermoreversible physical gelling systems consisting of poly(vinyl alcohol) and Congo Red (PVA/CR). The appearance of speckles, i.e., random fluctuations in the scattered intensity with respect sampling points, appeared exclusively in the gel state, i.e., $T < T_{gel}$ and $C_{PVA} > C_{PVA,gel}$. This indicates a similar type of frozen inhomogeneities is present in physical gels as well as in chemical gels. The intensity correlation function obtained by dynamic light scattering (DLS) was well fitted by a two-term function, which consists of a fast mode with a single-exponential function and a slow mode with a stretched exponential function (for sols) or a power law function (for gels). The ensemble-average scattered intensity, $\langle I \rangle_E$, was found to be a decreasing function of temperature. The decomposition of the fast mode gave information about thermal concentration fluctuations, $\langle I_F \rangle_T$, and the correlation length, ξ. The variations of ξ with C_{PVA} exhibited a divergence at $C_{PVA,gel}$, while that with T was monotonic across T_{gel}. The variations of the stretched exponent, β, the power-law exponent, n, and ξ are found to be different between the temperature-induced and concentration-induced transitions. This is due to the fact that the connectivity-correlation transition takes place more or less at the same time as the space-correlation transition in the case of the concentration-induced transition. On the other hand, the characteristic time for the slow mode, τ_{slow}, seems to be more sensitive to the connectivity-correlation transition than β as well as n since τ_{slow} diverges in both types of transition. The physical implementation of these findings was given in terms of the site-bond percolation model.

Acknowledgment. This work is partially supported by the Ministry of Education, Science, Sports, and Culture, Japan (Grant-in-Aid, 11305067 and 12450388). Thanks are due to the Cosmetology Research Foundation, Tokyo, for financial assistance. F.I. acknowledges the Research Fellowship of the Japan Society for the Promotion of Science for Young Scientists.

References and Notes

(1) Shibayama, M.; Morimoto, M.; Nomura, S. *Macromolecules* **1994**, *27*, 5060.
(2) Shibayama, M.; Moriwaki, R.; Ikkai, F.; Nomura, S. *Polymer* **1994**, *26*, 5716.
(3) Skouri, R.; Schosseler, F.; Munch, J. P.; Candau, S. J. *Macromolecules* **1996**, *28*, 197.
(4) Rubinstein, M.; Colby, R. H.; Dubrynin, A. V.; Joanny, J. F. *Macromolecules* **1996**, *29*, 398.
(5) Nisato, G.; Skouri, R.; Schosseler, F.; Munch, J.-P.; Candau, S. J. *Faraday Discuss.* **1995**, *101*, 133.
(6) Kabra, B. G.; Gehrke, S. H. *Polym. Commun.* **1991**, *32*, 322.
(7) Wu, X. S.; Hoffman, A. S.; Yager, P. *J. Polym. Sci., Part A* **1992**, *30*, 2121.
(8) Hirotsu, S. *Jpn. J. Appl. Phys. 37*, L284.
(9) Hirose, H.; Shibayama, M. *Macromolecules* **1998**, *31*, 5336.
(10) Ikkai, F.; Shibayama, M. *Phys. Rev. E* **1997**, *56*, R51.
(11) Shibayama, M.; Takata, S.; Norisuye, T. *Physica A* **1998**, *249*, 245.
(12) Shibayama, M. *Macromol. Chem. Phys.* **1998**, *199*, 1.
(13) Dainty, J. C. *Laser Speckle and Related Phenomena*; Springer-Verlag: Berlin, 1975.
(14) Pusey, P. N.; van Megen, W. *Physica A* **1989**, *157*, 705.
(15) Mallam, S.; Horkay, F.; Hecht, A. M.; Geissler, E. *Macromolecules* **1989**, *22*, 3356.
(16) Schosseler, F.; Skouri, R.; Munch, J. P.; Candau, S. J. *J. Phys. II* **1994**, *4*, 1221.
(17) Cohen, Y.; Ramon, O.; Kopelman, I. J.; Mizrahi, S. *J. Polym. Sci., Polym. Phys. Ed.* **1992**, *30*, 1055.
(18) Shibayama, M.; Norisuye, T.; Nomura, S. *Macromolecules* **1996**, *29*, 8746.
(19) Shibayama, M.; Ikkai, F.; Shiwa, Y.; Rabin, Y. *J. Chem. Phys.* **1997**, *107*, 5227.
(20) Ikkai, F.; Shibayama, M. *Kobunshi Ronbushu* **1998**, *55*, 632.
(21) Ikkai, F.; Shibayama, M. *Phys. Rev. Lett.* **1999**, *82*, 4946.
(22) Shibayama, M.; Ikkai, F.; Moriwaki, R.; Nomura, S. *Macromolecules* **1994**, *27*, 1738.
(23) Shibayama, M.; Ikkai, F.; Nomura, S. *Macromolecules* **1994**, *27*, 6383.
(24) Coniglio, A.; Stanley, H. E. *Phys. Rev. Lett.* **1979**, *42*, 518.
(25) Martin, J. E.; Wilcoxon, J. *Phys. Rev. Lett.* **1988**, *61*, 373.
(26) Ren, S. Z.; Shi, W. F.; Zhang, W. B.; Sorensen, C. M. *Phys. Rev. A* **1992**, *45*, 2416.
(27) Nystrom, B.; Roots, J.; Carlsson, A.; Lindman, B. *Polymer* **1992**, *33*, 2875.
(28) Martin, J. E.; Wilcoxon, J.; Odinek, J. *Phys. Rev. A* **1991**, *43*, 858.

(29) Joosten, J. G. H.; McCarthy, J. L.; Pusey, P. N. *Macromolecules* **1991**, *24*, 6690.
(30) Horkay, F.; Burchard, W.; Hecht, A. M.; Geissler, E. *Macromolecules* **1993**, *26*, 3375.
(31) Shibayama, M.; Fujikawa, Y.; Nomura, S. *Macromolecules* **1996**, *29*, 6535.
(32) Fujino, K.; Fujimoto, N. *Sen-i Gakkaishi* **1959**, *15*, 483.
(33) Ikkai, F.; Shibayama, M.; Nomura, S. *J. Polym. Sci., Polym. Phys. Ed.* **1996**, *34*, 939.
(34) Tanaka, T.; Hocker, L. O.; Benedek, G. B. *J. Chem. Phys.* **1973**, *59*, 5151.
(35) de Gennes, P. G. *Scaling Concepts in Polymer Physics*; Cornell University: Ithaca, NY, 1979.
(36) Freltoft, T.; Kjems, J. K.; Sinha, S. K. *Phys. Rev. B* **1986**, *33*, 269.
(37) Takeda, M.; Norisuye, T.; Shibayama, M. *Macromolecules* **2000**, *33*, 2909.
(38) Muthukumar, M. *Macromolecules* **1989**, *22*, 4656.

MA000563V